Vol. 23, n.°1, pp. 103-114, 2024
Revista UIS Ingenierías
https://revistas.uis.edu.co/index.php/revistauisingenierias

Microhardness Profile and Residual Stresses Evaluation in a Shot Peened SAE 5160H Steel

Evaluación del Perfil de Microdureza y Tensiones Residuales en un Acero Granallado SAE 5160H

Alexander Viloria-Estrada [1a], David Mantilla-Nova [1b], Daiver Alberto García-Salinas [2], Wilmar Barbosa [3], Claudia Constanza Palacio-Espinosa [4], Fidel Alfonso Romero [5], Dario Yesid Peña-Ballesteros [6], Jorge Guillermo Díaz-Rodríguez [7]

[1] Industrias Metálicas Asociadas S.A, Bogotá, Colombia. Emails: alexander.viloria@somosgrupo-a.com [a], david.mantilla@somosgrupo-a.com [b]
[2] CONFIPETROL, Bogotá, Colombia. Email: supervisorproducción.agrocascada@confipetrol.com
[3] UNIMINEX, Bogotá, Colombia. Emails: aprendizmecanico@uniminex.com
[4] Escuela de ciencias aplicadas e ingeniería EAFIT, Medellín, Colombia. Orcid: 0000-0001-8858-7165. Email: cpalac12@eafit.edu.co
[5] Universidad Pedagógica y Tecnológica de Colombia, Duitama, Colombia. Orcid: 0000-0002-5105-213X. Email: fidel.romero@uptc.edu.co
[6] Escuela de Ingeniería Metalúrgica y Ciencia de Materiales, Universidad Industrial de Santander, Colombia. Orcid: 0000-0002-6193-9535. Email: dypena@uis.edu.co
[7] Escuela de Ingeniería y Ciencias, Tecnológico de Monterrey, México. Orcid: 0000-0002-0479-4827. Email: jorgegdiaz@tec.mx

Received: 23 August 2023. Accepted: 30 December 2023. Final version: 9 March 2024.

Abstract

Shot peening (SP) is a surface cold hardening process used on metals to enhance life under cyclic stress. In this case, SP was applied to SAE5160H samples of steel quenched tempered in oil at 460 °C used for leaf springs. This study shows the residual surface stresses measured through X-ray diffraction (XRD) and the microhardness variation through the perpendicular-to-the-peened surface using a combination of metallographic preparation and Vickers microhardness (HVN). This combination of techniques makes possible measuring the SP effect in perpendicular-to-the-treated surface. A residual stress of -365.8 ± 78 MPa measured by XRD and a maximum microhardness of 525± at 92.7 HVN on the surface were obtained for the SP material. Alternatively, an average of 54.2 ± 54.3 MPa residual stress measured by XRD and 433 ± 39.5 HVN were obtained for the As-it-is samples. In addition, corrosion electrochemical potential tests showed that SP increases the corrosion potential, which makes this process undesirable if the SP component is exposed to aggressive environments. Moreover, the As-it-is samples presented not statistically significant HVN difference in the measured points. The combination of experimental techniques allows estimating hardness change in perpendicular-to-the treated surface separated by as little as 10 µm but with a simpler specimen preparation than other techniques such as XRD or strain gauges. Such a combination can be an alternative for estimating residual stresses through depth.

Keywords: Shot peening; Vickers microhardness; residual stress; SAE 5160; leaf springs.
ISSN Online: 2145 - 8456

How to cite: A. Viloria-Estrada, D. Mantilla-Nova, D. García-Salinas, W. Barbosa, C. Palacio-Espinosa, F. Romero, D. Peña-Ballesteros, J. G. Díaz-Rodríguez, "Microhardness Profile and Residual Stresses Evaluation in a Shot Peened SAE 5160H Steel," *Rev. UIS Ing.*, vol. 23, no. 1, pp. 103-114, 2024, doi: https://doi.org/10.18273/revuin.v23n1-2024009

Resumen

El granallado es una técnica de procesamiento de superficies en frío que en metales se usa para aumentar la vida bajo esfuerzos cíclicos. En este caso, el granallado se aplicó a muestras de acero SAE5160H (usado en resortes de ballesta) templado en aceite y revenido a 460 °C. En este estudio, se midieron esfuerzos residuales por medio de difracción de rayos X (DRX) y la dureza en la superficie perpendicular al tratamiento usando una combinación de pulido para metalografía y microdureza Vickers. Para el material procesado con granallado, las mediciones superficiales de DRX arrojaron una media de 365.8 MPa en compresión y una microdureza máxima de 525 ± 92.7 HVN. Por otro lado, para el material no procesado, se obtuvo una tensión residual positiva promedio de 54.2 MPa y 433 ± 39,5 HVN. Adicionalmente, ensayos de potencial electroquímico arrojaron que el granallado aumenta el potencial de corrosión, lo que hace este proceso indeseable si el componente granallado está expuesto a ambientes agresivos. La combinación de técnicas experimentales usadas permite estimar el cambio de dureza en la superficie perpendicular al granallado en mediciones discretas tan juntas como 10µm, pero con una preparación de probeta más simple que la requerida por otras técnicas como DRX o las galgas extensiométricas. Dicha combinación se puede ser alternativa para la estimación de esfuerzos residuales a través de la profundidad.

Palabras clave: Granallado; microdureza Vickers; SAE 5160H; esfuerzos residuales; resortes de ballesta.

1. Introduction

Several processes, such as thermochemical and thermomechanical heat treatment, coatings, and surface finishing, are used in the manufacture to improve the mechanical behavior of a component [1], [2]. For example, shot peening (SP) is a widely used technique that modifies surface mechanical properties, improving a component's fatigue response [3], [4]. It is standard practice for coil and leaf springs, such as the ones used in the automotive industry.

Fatigue life of components may be improved by inducing compressive residual stresses [1], [4]. The quantification of the effect of SP is done through methods such as Almen intensity [5], incremental drilling in blind holes according to ASTM - E837, or X-ray diffraction (XRD) [6]. However, these three techniques are shallow methods [4], [3]. Hernandez *et al*. [2] quantified these residual stresses by SP on AISI SAE 5160H steel using a combination of two techniques: electropolishing to remove material without affecting the hardness of the exposed material and XRD to measure residual stresses on each newly exposed surface. Although it gave good results, it is quite difficult to control the amount of material removed. Mičietová *et al.* [7] perfomed similar tests but for a 100Cr6 steel. Rodrigues *et al.* [8] measured residual stresses with strain gauges in slots at different depths treated as ellipses and fitting measurements to the Inglis stress field [9]. Jaramillo *et al.* [4] measured microhardness in a SAE 5160 steel subjected to SP, but only at the superficial level. Muñoz *et al.* [10] measured hardness in an SAE 306 steel subjected to deep rolling. Other authors have evaluated residual stresses left by SP with XRD, [11] in a 50CrMnMoVNb steel, [12] for a 18CrNiMo7-6, and [13] enhanced metal fatigue life by a combination of ultrasound impact and laser beam. Finally, Aguado *et al.* [14] recently proposed an arbitrary function that describes the optimal SP profile to improve the fatigue response of a component.

On the other hand, the requirement for leaf spring is the steel grade which must have sufficient hardenability for the grain size to ensure a completely martensitic structure throughout the section. The non-transformation in martensite produces lower fatigue endurance [15], [16]. The SAE 5160H steel is suitable for the fabrication of leaf springs. Its chemical composition can be seen on Table 1.

Table 1. Chemical composition of SAE 5160

C	0.56 - 0.64
Mn	0.75 - 1
Cr	0.7-0.9
Si	0.15- 0.30
P	≤0.035
S	≤ 0.04
Fe	Bal

On the other hand, the Vickers microhardness (HVN) can perform localized measurements with indentations as small as 25 µm [17] or even in new manufacturing process, such as Additive Manufacturing [18]. López-Crespo *et al.* [19] recently mapped the shape and size of the plastic zone under mixed-mode loading using the technique. They also found the results are independent of the indentation force. The article shows how the hardness of SAE 5160H steel, in the As-it-is and with shot peening conditions, varies through depth.

Furthermore, the method used here shows that it is possible to estimate the penetration of residual stresses by shot peening through the depth. A comparison of residual surface stresses by XRD and through depth by microhardness performed by cutting the samples in the cross-section is also presented.

2. Theoretical Foundation

2.1. Fatigue

Mechanical components are usually exposed to fluctuating stresses that produce nucleation of micro-fractures, which generate catastrophic failures when propagated over time [1]. This failure mode is called fatigue. There are three methods for estimating fatigue failure: stress-life, or S-N, which is responsible for predicting life for more than 10,000 cycles [1]; deformation life, Ɛ–N, or low cycle fatigue, for up to around 10,000 cycles [20]; and the da/dN method that is based on fracture mechanics and aims to predict service life in the presence of cracks [21], [22]. Moreover, it can be stated that the vast majority of components are designed with the S-N method [1], i.e. leaf springs are designed for lives of at least 100,000 cycles [3], [16].

2.2. Shot peening and Almen intensity

This cold process consists of impacting a surface with high-speed particles (between 20 and 120 m/s) to increase its hardness [3] to generate superficial plastic deformations and residual compression stresses, affecting only a thin layer. (0.1 to 0.5mm) [23]. In automotive components, i.e., leaf springs subjected to bending stresses, a beneficial effect is generated in the area subjected to positive stresses [4]. This treatment is commonly applied to engineering components that have complex geometry [1], [2] or are subjected to highly localized fluctuating stresses that can suffer from fretting [4], [23]. Shot peening is fast and suitable for mass production [1], [2].

On the other hand, shot peening can negatively impact the behavior of metals in corrosive environments since it decreases the potential for degradation of the passive layer [1]. Additionally, non-significant changes in AISI/SAE 5160 steel fatigue behavior have been reported when alternate bending tests were performed at three-point bending [4] but significant changes in low-carbon steels were reported under aggressive environments [24].

Furthermore, the Almen intensity measures the energy transmitted by the impact to the processed component [2], [24]. This scale measures the deflection of the arc formed in a normalized SAE 1070 steel strip when the pellets impact only one face. The procedure for this measurement is standardized by the SAE 442 [25] and SAE J443 [5] standards. The parameters of the shot peening process are material and diameter of the pellets, angle of the jet, distance from the jet to the surface, air pressure, exposure time, and shot flow [3], [23]. The surface appearance of a sample subjected to SP can be seen in Figure 1. Despite having a roughness that could favor crack initiation, the compressive stress induced by deformation generates beneficial behavior under an alternating load.

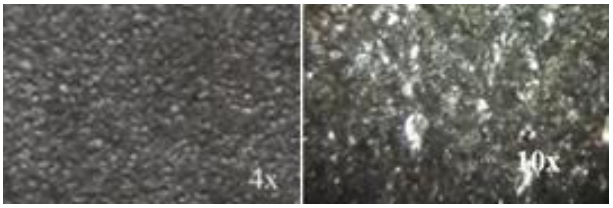

Figure 1. SP surface appearance, a) 4X; b) 10X. Source: [24].

One can place a standard metal strip next to the to-be-treated component to quantify the shot peening. The strip forms an arch, and its height, *H*, is measured. By plotting the deflection *H* of the arc formed against exposure time, a curve is generated, described by a parabola that opens towards the time axis. Therefore, increasing the exposure does not generate a more significant change in the curvature or residual stresses. Ideal shot peening is achieved when doubling the shot blast exposure time *t* results in only an increase in arc deflection, *ΔH*, which does not exceed 10%. This is known as the saturation curve [25] and can be seen in Figure 2.

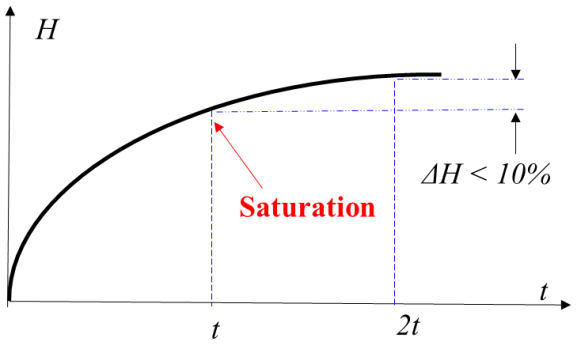

Figure 2. Schematic of the saturation curve. Source. Adapted from [25].

2.3. Shot peening and Almen intensity

Residual stresses are internal stresses that remain in a solid material after the action that originated them has ceased [26]. These stresses can occur due to a variety of

mechanisms, including cyclic plastic deformations [21], [22], elevated temperature gradients [20] or microstructural changes (i.e., phase transformation) [1]. It is a common but generally undesirable occurrence.

In a sample subjected to bending, the stress changes linearly with distance from the neutral axis. The imposed residual stress leaves compression closer to the surface but creates a tension zone to balance forces. The net stress is the superposition of applied and residual stress represented by the red dashed line in Figure 3.

X-ray diffraction (XRD) is based on Bragg's Law to determine the diffusion between atoms in crystalline materials, which allows such separation to act as diffraction gratings and lead to the generation of patterns that can be characterized [3]. The procedure for establishing residual stresses by XRD is described in ASTM E2860 [6]. The XRD technique allows measurements of variations in the parameter of the crystal lattice to calculate residual stresses.

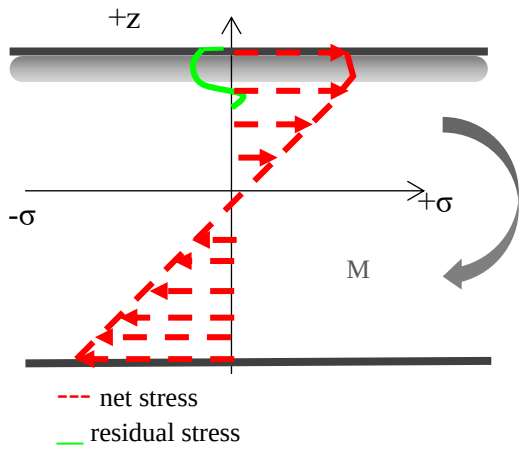

Figure 3. Schematics stress after SP Source: authors.

On the other hand, the blind hole technique, standardized by ASTM E837 [27], is based on the principle that stresses on free surfaces are zero. A strain gauge placed on a surface measures strain (ε_{xx}, ε_{yy}, ε_{xy}), and by making incremental perforations right in the center of the rosette that is formed due to the location of the gauges, strains away from the surface can be measured to a depth that can reach up to 15 mm [8].

Recently, Aguado *et al.* [14] presented a model based on the sinusoidal decay function that described the residual stress profile to minimize fatigue crack growth in a component. It is shown in equation (1).

$$\sigma_{res} = A\, exp^{-\lambda z}\, cos(\omega z + \theta) \qquad (1)$$

where A, λ, θ, and ω are constants to calibrate for each component, and z is the coordinate from the treated surface to the center of the component. An example of two theoretical residual stress profiles, called σ_1 and σ_2, obtained from equation (1) and using arbitrary constants is shown in Figure 4, in which the vertical axis is normalized residual stress. Such profiles exhibit a similar shape of what Hernandez *et al.* [3] measured by XRD and electropolishing. Recently, [7] reported similar residual stresses profiles for a heat-treated 100Cr6 steel subjected to different cutting speeds as well for a 15-5PH [28] subjected to compressive stress by roller burnishing.

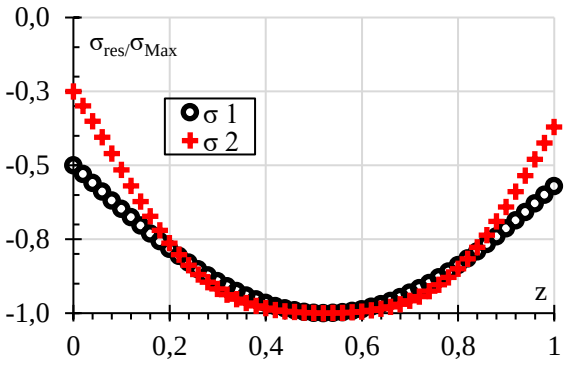

Figure 4. Examples of distribution of residual stress profiles according to equation (1), [14]. Source: authors.

The variation of the potential and current density of the anodic and cathodic curves should be linear at the Tafel slopes, intersecting at the point E_{corr}/i_{corr}. However, there are linear deviations in the vicinity of E_{corr}. These curves have regions with a linear ratio between the potential and the logarithm of the current density, an area called the Tafel region [18]. Figure 5 shows a portion of the curves obtained by applying a different potential to E_{corr}. It can be seen that the closer one gets to the value of E to that of E_{corr}, the value of i_{corr} tends to zero.

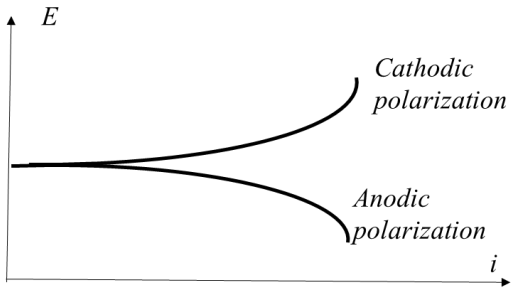

Figure 5. Schematics of corrosion potential curve. Source: authors.

3. Materials and methods

SAE 5160H steel samples with and without shot peening (SP and As) were prepared and cut perpendicularly in a Buehler IsoMet 1000 precision metallographic saw. First, the samples were prepared according to ASMT E466: roughed in a rotational polisher with the abrasive paper number 60, gradually decreasing the particle size until 1500. Then polishing was performed with 1 µm alumina. Finally, the samples were attacked with 5% Nital for 12 seconds. Through optical microscopy, it was verified that the microstructure corresponds to the heat treatment.

A Brucker UMT TriboLab™ micro-durometer was used using the Vickers scale and applying a 5N load. For each indentation, the lengths of diagonals d_1 and d_2 of the imprint left by the indenter were obtained, as outlined in Figure 6. Once the diagonals are obtained, the Vickers hardness (HV) is calculated with equation (2).

$$HV = 0.102\frac{2F\ sin\ \alpha}{d^2} \quad (2)$$

where F is the force applied in N, d the length of the diagonal in mm, and α the angle of the tip of the indenter, in this case, 136°.

Furthermore, the coordinates of each indentation on the cut and polished surface were measured following the coordinate system shown in Figure 7. The origin of the coordinate system is on the upper-left corner.

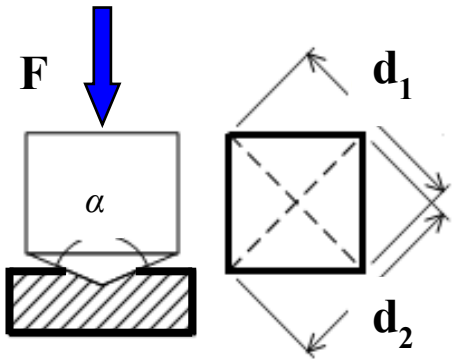

Figure 6. Schematic of a Vickers indentation and used nomenclature. Source: authors.

Due to the impossibility of measuring Vickers micro-hardness on the peened surface, Rockwell C (HRC) hardness measurements were made.

The scale conversion was done using ASTM E140.

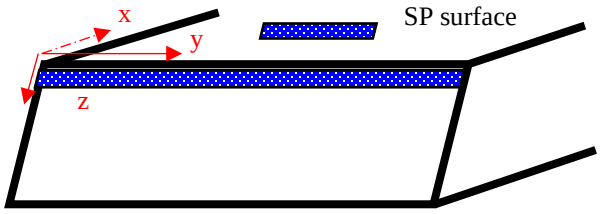

Figure 7. Microhardness measurement location schematic. Source: authors.

Furthermore, residual surface stresses were measured using a GNR-SpiderX® diffractometer model 2018 with a Cr X-ray tube.

Finally, SP and As-it-is samples were tested in an electrochemical cell containing a 3.5% weight Cl solution. The corrosion potential was measured by a Gamry 600 potentiostat using graphite as a counter electrode and Ag/AgCl as reference electrode.

4. Results and discussion

4.1. Microstructure

The microstructure for steel SAE5160H used in this study is shown in Figure 8a at 1000x and in Figure 8b at 2000x. A microstructure corresponding to tempered, thin, and acicular martensite is observed, corresponding to high hardness, while carbide precipitates can be seen in the dark regions.

The properties conferred to the AISI 5160H alloy are essential for the required applications in the automotive industry, allowing for the delay of fatigue crack nucleation that tends to occur on the surface.

Carbides are formed due to the segregation of elements such as chromium, vanadium, or molybdenum during the cooling and solidification process. The presence of carbides can have a significant impact on the mechanical properties of the steel, as they can contribute to strengthening and improving abrasion resistance.

4.2. XRD

Measurements were made at six points for two As-it-is samples and one SP sample, with 9 measurements at each point. A schematic of the location of the measured points is shown in Figure 9, where the roughness of a surface modified by SP can be appreciated. The samples were 10 mm wide x 15 mm long and 1/4" thick. The residual stress value at each point results from sweeping 9 measurements at different angles. Then the residual stress

result delivered at each point is the average of the 9 measurements made at different angles. Each measurement point is swept by X-rays at angles between -30º and +30º measured from a line perpendicular to the specimen. The goniometer makes 9 measurements: 4 before the zero angle, 1 at zero, and another 4 after the zero angle. The reliability of the measurement is above 80%. A positive stress means traction, whereas a negative value is compression.

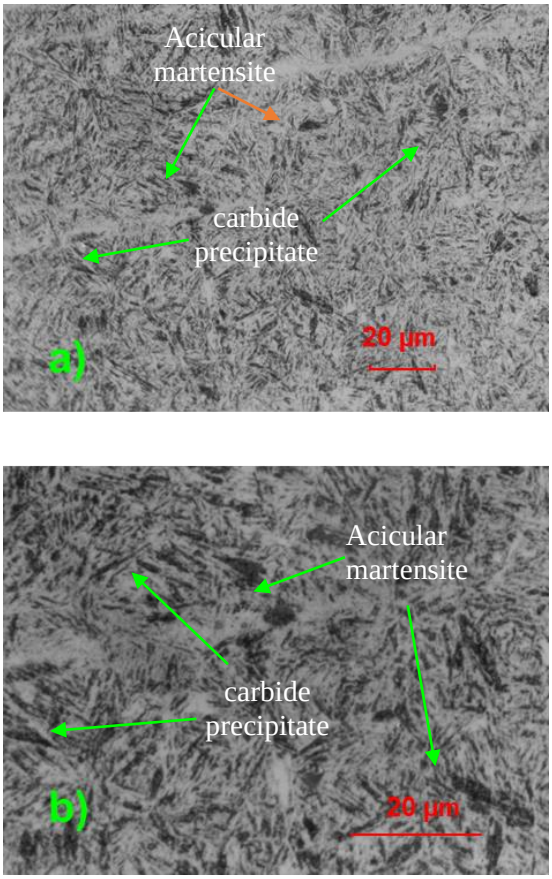

Figure 8. Microstructure of the steel used, a) 1000x, b) 2000x Source: authors.

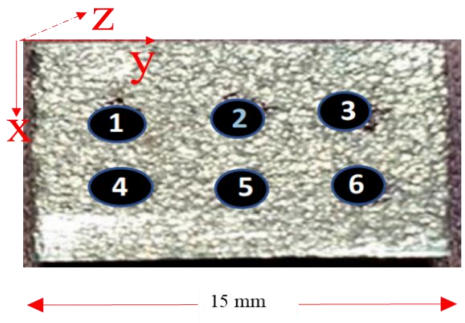

Figure 9. Location of XRD residual stress measurement points. Source: authors.

Figure 10 shows the absolute value of the surface residual stresses measured by the XRD technique. The sample with SP residual stresses presents residual compression stresses of average value -365.8 ± 78 MPa while the sample As-it-is presents average positive residual stresses of 54.2 ± 54.3 MPa. An increase in average compressive residual stress of 420 MPa on the As-it-is samples can be observed. Moreover, when comparing the residual surface stress with the flexural strength (2170 MPa), an increase of 16.8% is obtained, which is within the values accepted by the industry for the process [3], [16]. However, the XRD technique delivers results of residual surface stress. Therefore, the depth of this change and how these stresses vary are unknown.

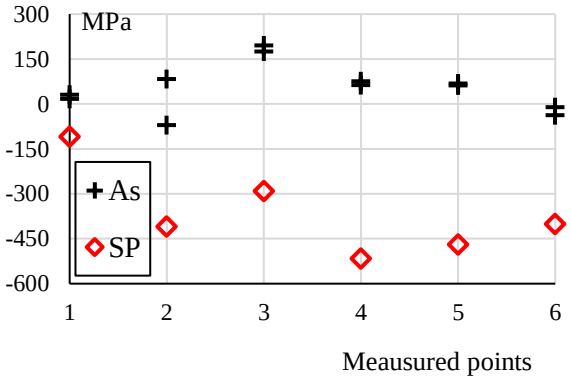

Figure 10. XRD residual stress per measured point, as described in Figure 9. Source: authors.

4.3. Microhardness

Figure 11 shows the Vickers microhardness results for a shot-peened sample taken at three measured depths (0.07, 0.17, and 0.27 mm) from the processed surface. HV values were estimated according to equation (2).

From the microhardness results, the average and standard deviation for each Z depth was calculated. Table 2 shows the average values of Vickers microhardness and standard deviation for samples with shot peening at the 4 distances measured. It is observed that in the SP sample, the HVN varies between 525 on the surface, reaching a minimum at 374 MPa at 0.07 mm and then recovering to 390 at 0.17 and 418 at 0.27 mm. [11]; The greatest increase occurs not at the surface but at a depth of about 0.3 mm from the peened surface.

From the microhardness results, the average and standard deviation for each Z depth was calculated. Table 2 shows the average values of Vickers microhardness and standard deviation for samples with shot peening at the 4 distances measured. It is observed that in the SP sample, the HVN varies between 525 on the surface, reaching a

minimum at 374 MPa at 0.07 mm and then recovering to 390 at 0.17 and 418 at 0.27 mm [11]; The greatest increase occurs not at the surface but at a depth of about 0.3 mm from the peened surface.

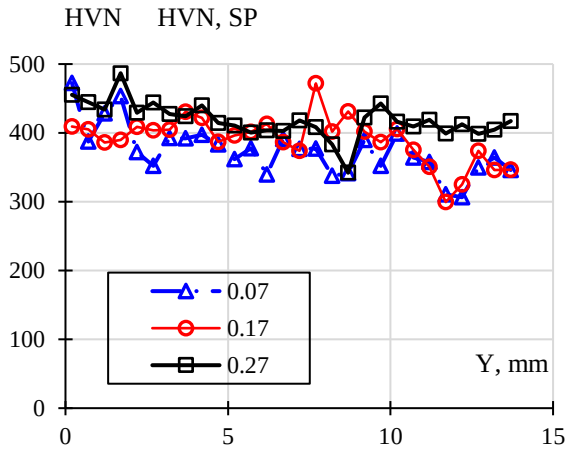

Figure 11. Vickers microhardness measured at different edge depths for a shot-peened sample (SP). Source: authors.

From the microhardness results, the average and standard deviation for each Z depth was calculated. Table 2 shows the average values of Vickers microhardness and standard deviation for samples with shot peening at the 4 distances measured. It is observed that in the SP sample, the HVN varies between 525 on the surface, reaching a minimum at 374 MPa at 0.07 mm and then recovering to 390 at 0.17 and 418 at 0.27 mm [11]; The greatest increase occurs not at the surface but at a depth of about 0.3 mm from the peened surface.

Table 2. Average HVN and standard deviation values for SP samples

HVN	SD	Z [mm]
525.6	92.7	0
374.1	36.9	0.07
390.5	34.5	0.17
418.2	25.8	0.27

Source: authors.

On the other hand, Table 3 shows the average values of Vickers microhardness and standard deviation for samples without shot peening at the 4 distances measured. It is observed that the HVN varies between 433 and 344. Despite showing a couple of extreme points in both samples, the SD is between 39.5 and 48.2 HV (9.1 to 14%) for As-it-is and between 92.7 and 25.8 HVN (17.6 to 6.2%) for the SP sample.

Although the literature cites SP as a heterogeneous process, we see a variation in the effect of the process from the dispersion of data.

Table 3. Average Vickers microhardness and standard deviation values for samples without shot peening

HVN	SD	Z [mm]
433	39.5	0
344.1	48.2	0.16
370.1	47.1	0.26
352.7	40.6	0.36

Source: authors.

Table 3, SP sample, shows more homogeneous values of Vickers micro-hardness compared to the values observed in Table 2, As-it-is sample, which is also reflected in the SD of the measurements. This may be related to the compression effect of the surface when treated with SP, confirmed by the results in Figure 10, where the sample subjected to the SP process showed residual compression stresses. The drop in some Vickers microhardness values observed in the As-it-is sample of Figure 12 may be a consequence of the effects of the microstructure on the measured points since areas of retained austenite are observed that are typically softer than the martensite that is also present in the microstructure, see Figure 8.

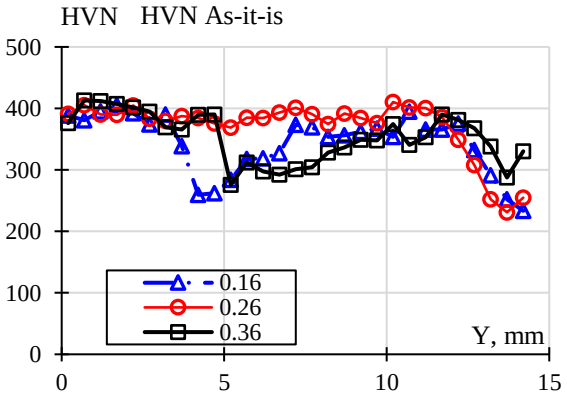

Figure 12. Vickers microhardness at different edge depths for as it is (As) sample. Source: authors.

Moreover, Figure 13 shows an example of an indentation imprint. The photograph is taken at 40x with a field view of 61.70 x 176.8 µm. The imprint´s symmetric shape is appreciated, noting that it is much larger than the size of the microstructural features shown in Figure 8.

Hence, the measured microhardness is not affected by the local microstructure.

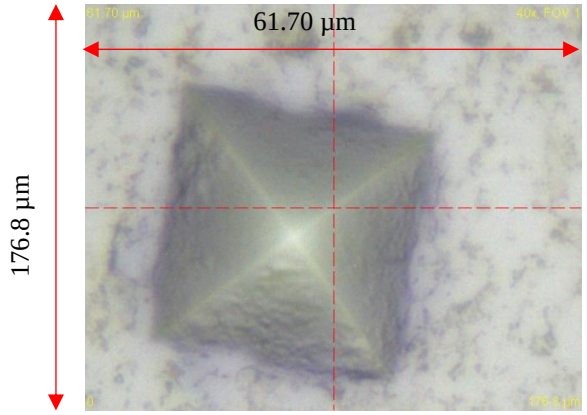

Figure 13. Example of the imprint of the Vickers micro-indenter. Source: authors.

On the other hand, the variability of the diagonal measurement for each measured depth is shown in Table 4. For the As-it-is sample, the SD between diagonals ranges between 0.48 and 0.71% of the average hardness of each diagonal, while in the SP sample, the SD between diagonals ranges from 0.21 to 1.06% of the average hardness of each diagonal.

To establish whether there is a significant difference between the hardness measurements taken at different depths, see the nomenclature in Figure 7, a null hypothesis (H_0: the hardness averages are equal) and an alternative hypothesis (H_1: there are significant differences in the hardness averages) were proposed for each sample. The analysis of variance (ANOVA) showed that the null hypothesis (H_0) is accepted with a 96.89% probability for samples without shot peening (As). On the other hand, the ANOVA indicated that the null hypothesis H_0) should be rejected for SP samples, giving a probability of 83.95%. This indicates that the hardness does not change with the depth in the As-it-is samples, unlike in the SP samples. One might think that the lateral restriction imposed by the thickness influences how the hardness measurement might be affected. However, according to the ANOVA, that does not occur. That effect might be attributed to the shallow imprint not being affected by thick or thin surroundings.

Finally, Figure 14 shows results for electrochemical tests. For the As-it-is samples the potential is -620 mV, while for SP is -750 mV. Therefore, from the thermodynamics point of view, the SAE 5160H steel with SP has a higher corrosion rate because the surface treatment performs a plastic deformation on the surface of the material, generating empty spaces which are not impacted the pellets. These empty spaces act as interstices, in which agents that generate oxides lodge more easily. Thus, increasing the progressive degradation of steel by corrosive factors.

Table 4. Standard deviations of diagonals for samples.

Z [mm]	SD d_1	SD d_2
As		
0.16	2.45	2.31
0.26	2.33	2.23
0.36	1.82	1.69
SP		
0.07	2.67	3.98
0.17	2.07	1.13
0.27	1.09	0.89

Source: authors.

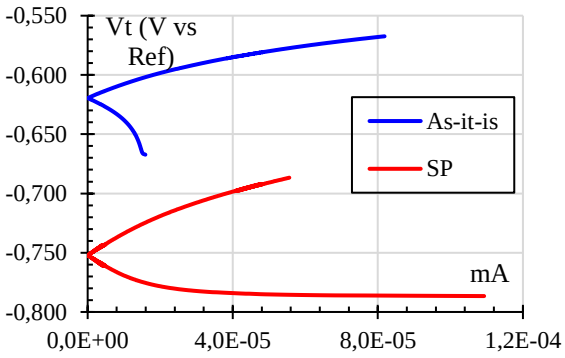

Figure 14. Corrosion electrochemical potential results. Source: authors.

4.4. Discussion

The XRD makes it possible to determine the residual surface stress, which is the difference between the surface strength and the permanent deformation imposed by an external process, such as compression by SP. However, [3] described how the heat treatment might induce decarburization, leading to lower strength at depths up to 1 mm. Hence, XRD to measure residual surface stress should not be used without knowledge of material processing.

On the other hand, microhardness quantifies the strength of a material to be scratched or indented. Still, it does not necessarily lead to the direct determination of the material's mechanical strength, which is usually assessed by tensile tests. However, it is acceptable to estimate a material's strength from hardness measurements, such as ASTM E140. Therefore, hardness can be used to estimate the material's surface strength value. In this case, the measured HVN values are the combination of material

strength and changes introduced by shot peening and even sample preparation. In this case, samples were cut by EDM and polished, although an attempt was made to keep such modifications to a minimum, and a uniform effect was sought for the analyzed samples.

Consequently, to be able to compare residual stress by XRD with stresses estimated from microhardness and converted to stress according to accepted estimates (such as ASTM E140), the value of the material's ultimate strength to the residual stress measured by XRD should be added to identify the material's ability to withstand service loads.

Moreover, it is highlighted that the low standard deviation between the values of the two diagonals shows that their measurement was consistent and that the indentations were not affected by external agents such as microstructure or lack of rigidity due to proximity to free surfaces.

Because of the imposed stress profile under bending, the crack initiation occurs on the positively stress surface, the crack initiation time could be maximized by adopting a residual compressive stress profile on the surface of the treated part.

On the other hand, if crack propagation is the main contribution to the component's life, the residual stress profile should be designed so that the stress intensity factor governing fatigue crack growth [21] is as low as possible [14]. In the case of leaf springs, the maximum bending stress is located on the convex surface and decreases linearly towards the concave plane until reaching the neutral plane. Alternating bending preliminary tests showed little or no crack growth before component failure occurred. It has been shown that the SP compressive effect surpasses rugosity´s negative effects incrementing fatigue life [28], [29]. Therefore, choosing the option that maximizes the S-N span of the component makes sense.

Finally, Aguado *et al.* [14] recognized that a disadvantage of the proposed model is that constants have no physical meaning. From experimenting with the model, we found that the constant A is related to the initial amplitude of the residual stress, λ to the decay of the stress towards the minimum value, and ω and θ to the location of the minimum residual stress point. It remains open to establishing which variables of the peening process, or another surface hardening process, are related to the variables of the Aguado *et al.* model [11].

5. Conclusion

The procedure for evaluating microhardness and determining residual stresses by a non-destructive technique (XRD) made it possible to evaluate the effect of SP on the hardness of the material, as well as the possible impact of the microstructural characteristics of steel on microhardness. SP has a positive impact on the behavior of the analyzed metal by generating a surface with a higher hardness in relation to the surface hardness of the as-it-is material. Furthermore, the XRD technique delivers residual compressive stress results on the exposed surface, which confirms the result of the influence of the SP on the surface of the material.

It was found that XRD measurements show that the surface SP samples present residual stresses between -100 MPa and -500 MPa approximately, in contrast to the tension values of the As-it-is samples with mostly positive values (stress) ranging up to approximately 200 MPa.

The effectiveness of the peening process to create compression surfaces is evident, which represents an improvement in mechanical resistance when the component is subjected to cyclic loads, as reported in the literature. In this way, it is possible to define a procedure that allows parameterizing the peening processes in relation to the load the material is expected to withstand in service.

An increase in mechanical properties with depth and directionality was appreciated through microhardness. The highest increase in residual stress occurred not at the surface but at 0.3 mm deep from the peened surface. The Vickers microhardness measurement showed that in the sample with shot peening, the measurement varies from 525 at the surface, falls to 374 to 0.07 mm, and reaches a value of 418 HVN to 0.27 mm. The ANOVA showed statistically significant differences between the measurements at different depths. On the other hand, for the As-it-is sample, the microhardness varies between 433 and 344 HVN, and the ANOVA found no statistically significant differences in depth change.

Although SP delivers compressive residual stress results that are beneficial under service loads such as fatigue, the process may accelerate the corrosion initiation in a similar way as lamination augments strength but decreases corrosion resistance.

Funding acquisition

The authors acknowledge financial support from UPTC under project 2857.

Autor Contributions

A. Viloria-Estrada: Formal Analysis, Investigation, Writing – review & editing. D. Mantilla-Nova: Conceptualization, Investigation, Methodology, Validation, Writing – review & editing. D. García-Salinas: Conceptualization, Investigation, Methodology, Validation, Writing – review & editing. W. Barbosa: Conceptualization, Investigation, Methodology, Validation, Writing – review & editing. C. Palacio-Espinosa: Conceptualization, Investigation, Validation, Writing – review & editing. F. Romero: Formal Analysis, Investigation, Writing – review & editing. D. Peña-Ballesteros: Formal Analysis, Investigation, Writing – review & editing. J. G. Díaz-Rodríguez: Formal Analysis, Investigation, Writing – review & editing.

All authors have read an agreed to the published version of the manuscript.

Conflicts of Interest

The authors declare no conflict of interest.

Institutional Review Board Statement

Not applicable.

Informed Consent Statement

Not applicable.

Acknowledgements

The authors thank Ms. L. X. Arenas from the UIS metallography laboratory for the help in samples preparation and Mr. C. Calero for the help in taking the indentations. F.

References

[1] J. T. P. Castro and M. Meggiolaro, *Fatigue Design Techniques*, Vol I, 3rd ed. Scotts Valley, CA, USA: CreateSpace, 2016.

[2] D. Kirk, "Quantification of shot peening coverage," *The Shot Peener, Mishawaka*, pp. 22–34, Jan. 2014.

[3] H. Hernández, A. Viloria, Y. Arango, A. Jiménez, H. Mendoza, J. Cadena, "Mejoramiento del proceso de granallado para resortes de ballesta utilizando medición de esfuerzos residuales por difracción de rayos X," *Revista Ingeniería e Investigación*, no. 56, pp. 33–40, 2004.

[4] H. E. Jaramillo, N. A. de Sánchez, J. A. Ávila, "Effect of the shot peening process on the fatigue strength of SAE 5160 steel," *Proc Inst Mech Eng C J Mech Eng Sci*, vol. 233, no. 12, pp. 4328–4335, 2019, doi: https://doi.org/10.1177/0954406218816349

[5] SAE, "SAE J443. Procedures for Using Standard Shot Peening Test Strip," *SAE International*, 2018. doi: https://doi.org/10.4271/J443_198401

[6] ASTM, "ASTM E 2860. Standard Test Method for Residual Stress Measurement by X-Ray Diffraction for Bearing Steels," 2012.

[7] A. Mičietová, M. Čilliková, R. Čep, B. Mičieta, J. Uríček, M. Neslušan, "An Investigation of Residual Stresses after the Turning of High-Tempered Bearing Steel," *Machines*, vol. 12, no. 2, p. 139, 2024, doi: https://doi.org/10.3390/machines12020139

[8] L. D. Rodrigues, J. L. F. Freire, R. D. Viera, "Desenvolvimento e avaliação experimental de uma nova técnica para medição de tensões residuais," *Revista Matéria UFRJ*, vol. 16, no. 4, pp. 842–856, 2011.

[9] C. Inglis, "Stresses in Plates Due to the Presence of Cracks and Sharp Corners," *Transactions of the Institute of Naval Architects*, vol. 55, pp. 219–241, 1913.

[10] J. Muñoz-Cubillos, J. J. Coronado, S. A. Rodríguez, "Deep rolling effect on fatigue behavior of austenitic stainless steels," *Int J Fatigue*, vol. 95, pp. 120–131, Feb. 2017, doi: https://doi.org/10.1016/j.ijfatigue.2016.10.008

[11] B. Xia et al., "Improving the high-cycle fatigue life of a high-strength spring steel for automobiles by suitable shot peening and heat treatment," *Int J Fatigue*, vol. 161, p. 106891, Aug. 2022, doi: https://doi.org/10.1016/j.ijfatigue.2022.106891

[12] Y. Li, P. Wei, X. Zhao, R. Zhu, J. Wu, H. Liu, "A novel approach of shot peening process parameters prediction with missing surface integrity data based on imputation method," *The International Journal of Advanced Manufacturing Technology*, May 2023, doi: https://doi.org/10.1007/s00170-023-11514-x

[13] S. A. Ojo et al., "Improving fatigue life of additively repaired Ti-6Al-4V subjected to laser-assisted ultrasonic nanocrystal surface modification," *Int J Fatigue*, vol. 173, p. 107663, 2023, doi: https://doi.org/10.1016/j.ijfatigue.2023.107663

[14] S. Aguado-Montero, J. Vázquez, C. Navarro, J. Domínguez, "Optimal shot peening residual stress profile for fatigue," *Theoretical and Applied Fracture Mechanics*, vol. 116, p. 103109, 2021, doi: https://doi.org/10.1016/j.tafmec.2021.103109

[15] E. H. Judd, *Spring Design Manual*. Warrendale PA: SAE, 1996.

[16] D. Mantilla, N. Arzola, O. Araque, "Optimal design of leaf springs for vehicle suspensions under cyclic conditions," *Ingeniare. Revista chilena de ingeniería*, vol. 30, no. 1, pp. 23–36, 2022, doi: https://doi.org/10.4067/S0718-33052022000100023

[17] M. Yetna N'Jock, D. Chicot, X. Decoopman, J. Lesage, J. M. Ndjaka, A. Pertuz, "Mechanical tensile properties by spherical macroindentation using an indentation strain-hardening exponent," *Int J Mech Sci*, vol. 75, pp. 257–264, Oct. 2013, doi: https://doi.org/10.1016/j.ijmecsci.2013.07.008

[18] D. G. Agredo-Diaz et al., "Evaluation of the corrosion resistance of an additive manufacturing steel using electrochemical techniques," *Revista UIS Ingenierías*, vol. 19, no. 4, pp. 213–222, 2020, doi: https://doi.org/10.18273/revuin.v19n4-2020018

[19] C. Lopez-Crespo, A. S. Cruces, S. Seitl, B. Moreno, P. Lopez-Crespo, "Estimation of the Plastic Zone in Fatigue via Micro-Indentation," *Materials*, vol. 14, no. 19, p. 5885, Oct. 2021, doi: https://doi.org/10.3390/ma14195885

[20] A. D. Pertuz-Comas, O. A. González-Estrada, E. Martínez-Díaz, D. F. Villegas-Bermúdez, J. G. Díaz-Rodríguez, "Strain-Based Fatigue Experimental Study on Ti–6Al–4V Alloy Manufactured by Electron Beam Melting," *Journal of Manufacturing and Materials Processing*, vol. 7, no. 1, p. 25, Jan. 2023, doi: https://doi.org/10.3390/jmmp7010025

[21] M. Vormwald, Y. Hos, J. L. F. Freire, G. L. G. Gonzáles, J. G. Díaz, "Variable mode-mixity during fatigue cycles – crack tip parameters determined from displacement fields measured by digital image correlation," *Frattura ed Integrità Strutturale*, vol. 11, no. 41, pp. 314–322, Jun. 2017, doi: https://doi.org/10.3221/IGF-ESIS.41.42

[22] J. G. Díaz-Rodríguez, G. L. Gonzales, J. A. Ortiz Gonzalez, J. L. de F. Freire, "Analysis of Mixed-mode Stress Intensity Factors using Digital Image Correlation Displacement Fields," in *Proceedings of the 24th ABCM International Congress of Mechanical Engineering*, ABCM, Ed., Curitiba: ABCM, 2017. doi: https://doi.org/10.26678/ABCM.COBEM2017.COB17-0684

[23] S. Vantadori, A. Zanichelli, "Fretting-fatigue analysis of shot-peened aluminium and titanium test specimens," *Fatigue Fract Eng Mater Struct*, no. September, p. ffe.13367, Oct. 2020, doi: https://doi.org/10.1111/ffe.13367

[24] F. Romero, A. Pertuz, and J. G. Diaz, "Fatigue study on AISI/SAE 1015 steel with shot peening under corrosive environments," *J Phys Conf Ser*, vol. 1938, no. 1, p. 012005, May 2021, doi: https://doi.org/10.1088/1742-6596/1938/1/012005

[25] SAE, "SAE J442. Test Strip, Holder, and Gage for Shot Peening," 2013. doi: https://doi.org/10.4271/J442_201302

[26] J. G. Díaz-Rodríguez, "Comparison of stress separation procedures. experiments versus theoretical formulation," *Engineering Solid Mechanics*, vol. 10, no. 2, pp. 153–164, 2022, doi: https://doi.org/10.5267/j.esm.2022.1.003

[27] ASTM, "ASTM E 837. Standard Test Method for Determining Residual Stresses by the Hole-Drilling Strain-Gage Method," 2013.

[28] F. Valiorgue et al., "Influence of residual stress profile and surface microstructure on fatigue life of a 15-5PH," *Procedia Eng*, vol. 213, pp. 623–629, 2018, doi: https://doi.org/10.1016/j.proeng.2018.02.058

[29] B. Reggiani, G. Olmi, "Experimental Investigation on the Effect of Shot Peening and Deep Rolling on the Fatigue Response of High Strength Fasteners," *Metals (Basel)*, vol. 9, no. 10, p. 1093, 2019, doi: https://doi.org/10.3390/met9101093